Leonard MELCESCU[1], Mihail V. CISTELECAN[2], Ovidiu CRAIU[1], Mihail POPESCU[2]

POLITEHNICA University of Bucharest (1), Research Institute for Electrical Machines of Bucharest (2)

Numerical Analysis of Claw Pole Synchronous Machine with Hybrid Contactless Excitation

Abstract. *The paper presents the analysis of a 3-D numerical model developed for a new claw pole synchronous machine with hybrid and contactless excitation. The main field is produced by NdFeB permanent magnets placed in the rotor, and by two fixed field coils mounted inside machine shields and fed from a controlled DC current supply. The complex structure of the claw-pole magnetic circuit required usage of a 3 D FEM model and a scalar potential formulation, in order to reduce computing time and memory. The no-load and magnetization characteristics and the e.m.f. time dependence have been calculated.*

Streszczenie. *Artykuł przedstawia analizę trójwymiarowego modelu numerycznego nowej maszyny synchronicznej z biegunami pazurowymi z hybrydowym i bezkontaktowym wzbudzeniem. Złożona struktura maszyny wymaga użycia modelu trójwymiarowego MES i potencjału skalarnego. (**Analiza numeryczna maszyny synchronicznej ze wzbudzeniem hybrydowym i bezkontaktowym**).*

Keywords: hybrid excitation synchronous machine, finite element method, permanent magnets.
Słowa kluczowe: maszyna synchroniczna ze wzbudzeniem hybrydowym, metoda elementów skończonych, magnesy trwałe.

Introduction

Various types of electrical machines providing increased power density and operating within a wide range of speeds have been produced during the last years. Noteworthy are those synchronous machines with hybrid excitations that have main field produced by both PM and field coils. Different configurations of various hybrid synchronous machines used in vehicle propulsion [2], high speed machine tools applications [3], or as automotive generators [4-7] have been designed and thoroughly analyzed.

Hybrid synchronous machines can be used equally as motors and generators. The hybrid excitation combines the advantages of using permanent magnets that allow for high power densities, and the possibility of controlling the main field through excitation current. Controlling the main field allows machine to operate at power factor one. Hence electronic equipment connected to the induced windings transfers only active power and can be reduced in size.

Analyzing these hybrid machines, and particularly the way the two exciting systems are influencing one another, has been done with simpler 2D numerical models [7,8], but also availing of more complex, 3D models [9-11]. This paper presents a 3D model analyzing the main field into a hybrid synchronous machine with new design [1].

Topology of the hybrid synchronous machine

The studied experimental model is a three phase hybrid synchronous machine with $Z = 36$ stator slots and $2p = 10$ poles, with axial symmetry against median cross section, Fig. 1. a-b. The rotor, which is the inductor, is composed of two symmetrical modules, each made of two ferromagnetic parts with claw poles that surround the permanent magnets. The ring shaped PM are magnetized along their axial direction. The claw poles of the inner parts exceed the axial length of the stator. The field coils are placed at the end sides of the rotor, embedded into two ferromagnetic cylinders mounted on the stator, Fig. 1. c-d. Each ferromagnetic cylinder has a gutter to allow the tips of the claw poles to rotate freely. The magnetic field generated by each field coil closes through one outer ferromagnetic part, the longer claw poles, the stator yoke and then through the shorter claw poles. Therefore, the magnetic field passes through three air gaps: the axial-radial air-gap between the long claw poles and the outer ferromagnetic piece, the air-gap between the stator and the rotor and the air-gap between the shorter claw poles and the outer ferromagnetic piece.

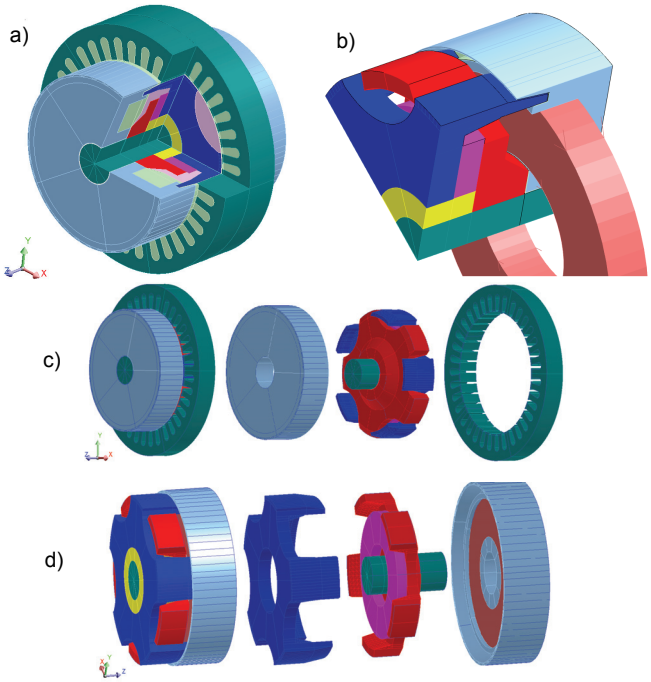

Fig.1. The claw pole synchronous machine with hybrid contactless excitation: a. General view; b. Magnetic circuit of half machine; c. Structure of half inductor; d. Hybrid excitation system detail

The machine has the following rated data when operates as a generator: S_n = 750 VA, U_n = 120 V, I_n = 3.6 A, $\cos(\varphi_n) = 1$, n_n = 1200 rpm, I_{fn} = 0 A. The main dimensions and characteristics of the experimental model are:

Table 1. Specification of analysed hybrid synchronous machine

Outer diameter of stator lamination:	185 mm
Inner diameter of stator lamination:	129 mm
Stator stack length:	50 mm
Total magnetic iron length of the inductor:	127 mm
Air gap size:	0.7 mm
Number of stator slots:	36
Turns per phase:	324
Winding connection:	Star
PM dimensions:	Φ100/Φ50/8 mm
PM performance (NdFeB quality):	Br = 1,15 T Hc = 8360 A/cm.

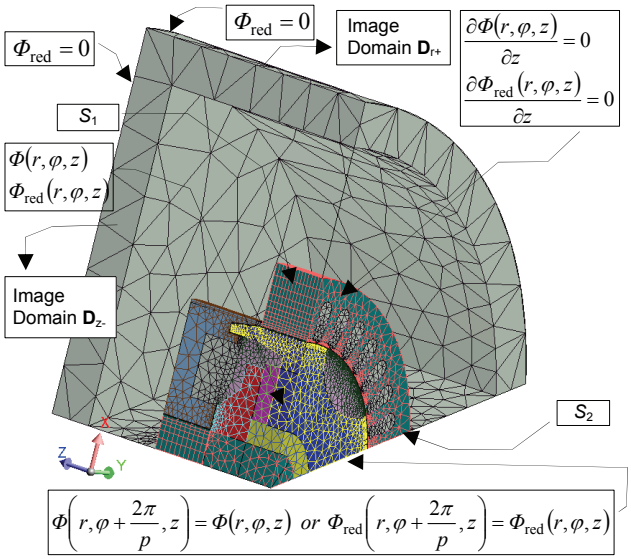

Fig. 2. Computation domain and boundary conditions

FEM Analyses

The complex structure of the magnetic circuit and the presence of the axial and radial field required a 3D numerical model. A non-linear model based on the magnetic scalar potential formulation has been generated in Flux 3D, a FEM professional software produced by CEDRAT [12]. The magnetic field distribution has been computed and from that the magnetization characteristic and the no-load characteristic of the generator were determined. Solutions have been computed when magnetic flux was produced by the PM alone, then by the excitation coils, and last by both. The time variation of the e.m.f. induced in the stator windings has been computed by rotating the rotor over 2 poles.

In order to reduce the number of finite elements, mesh nodes, and thus computing time, a formulation based on total scalar, Φ, and reduced scalar magnetic potential, Φ_{red}, has been used. The total scalar potential Φ applies in the regions occupied by permanent magnets and iron cores. Taking into account that in these regions the current density **J** is zero, the magnetic field **H** is non-rotational and respects the equation:

$$\mathbf{H} = -\operatorname{grad} \phi \,. \tag{1}$$

The equation above together with $B = f(H)$ dependence and Maxwell's equations yield the following governing equation resolved by means of FEM:

$$\operatorname{div}[-\mu(\mathbf{H}) \operatorname{grad} \phi + \mathbf{B}_r] = 0 \,, \tag{2}$$

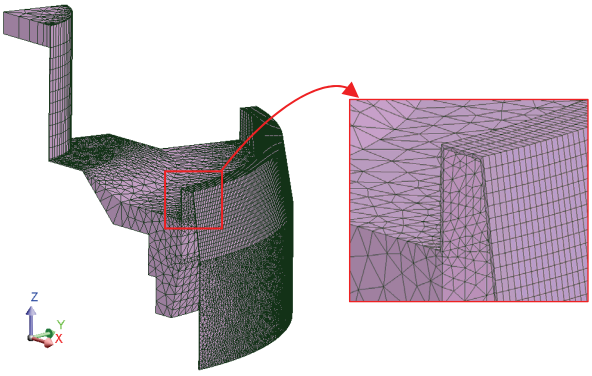

Fig. 3. The airgap mesh detail

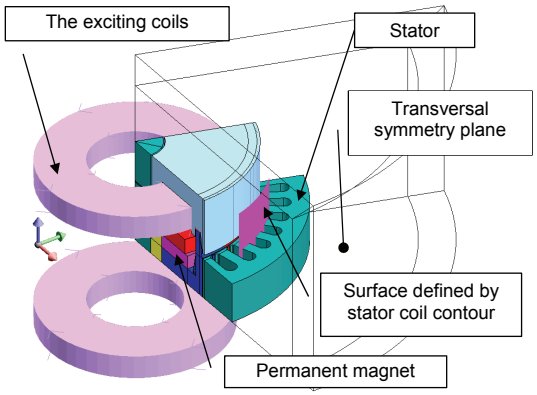

Fig. 4. The excitation field sources

where $\mathbf{B}_r$ is the remnant magnetic field density and μ the magnetic permeability. The reduced scalar potential Φ_{red} is used in air regions and in the coils. The potential is computed with respect to $\mathbf{H}_J$ so that:

$$\mathbf{H} = \operatorname{grad} \phi_{red} + \mathbf{H}_J \,, \tag{3}$$

where $\mathbf{H}_J$ is the source field produced by non-meshed conductors and is determined using Biot-Savart relation.

The computing domain has been reduced according to machine's geometrical symmetry and magnetic field periodicity. This is the volume delimited by the symmetry axial sections of two consecutive poles of same polarity and machine's mid cross section, Fig. 2. The rotor position relative to stator was chosen in such a way that the two axial sections that pass through the middle of the poles, cross the rotor teeth symmetrically, leaving same tooth width on both left and right side of rotor section. The geometrical periodicity has been implemented on boundary surfaces S_2 and S_1. On the mid cross section plane, the magnetic field has only a tangential component.

In order to determine the e.m.f. time dependence, successive numerical solutions were computed using a circuit-field model for successive rotor displacements. The rotor movement was modeled using a slip surface placed in the geometrically complex air-gap area, Fig. 3.

The sources of the magnetic field are the permanent magnets and two current supplied field coils. Although not shown in the model, a second excitation coil was considered in order to respect the symmetry condition against the transversal plane, as shown in Fig. 4.

The computation domain was divided in 393 969 first order volume elements, 138 055 surface elements and 12 793 line elements, with a total of 103 016 nodes. The field problem was solved for magneto-static regime and transient magnetic regime, respectively. Computing time to solve one non-linear static problem was about 2 minutes using a server equipped with Intel Xeon Quad Core processor at 2.5 GHz, and 16 GB of RAM memory.

Numerical and Experimental Results

Although analyzing electrical machines using complex numerical methods is time consuming and requires special skills and powerful computers, these methods are a powerful and effective tool for designers. First, the numerical analysis offers local information about field values, local stress and other data which is not available by direct measurement. Then, by additional postprocessing, the numerical model can provide also global, integrated values, and their time dependences, which can be compared directly with the experimental determinations.

In this particular case, in order to study the main field in the hybrid excited machine, different numerical models

were used. The magnetic fields produced by PM and by field coils were determined separately. The magnetic field distribution is presented in Fig. 5.a when produced by PM alone, and in Fig. 5.b when produced only by the field current (magnets were replaced by air). From comparing the two situations it is noticeable that the field produced by PM is stronger, while the magnetic field produced by the excitation coils is weaker and it is used only for regulating the total flux in the machine, either as additional or differential compound. Fig. 5.a shows that not all magnetic flux produced by PM reaches the stator, a small part closes through the ferromagnetic cylinder surrounding the field coil. This leakage flux causes an offset in the radial component of the magnetic flux density time variation (the negative pick is larger than the positive pick, as can be seen in Fig. 6.a).

The area with magnetic saturation and greater magnetic induction in Fig. 5.b represents the closing paths of the field produced by the field current. The magnetic flux density inside the poles is smaller in this second case, and produces a reduced field in the air-gap, as seen in Fig. 6.b.

When both field sources are present (PM and field current), the magnetic field in the air-gap is obtained by either adding the two fields (additional compound, Fig. 5.c), or by subtracting them (differential compound, Fig. 5.d). In Fig. 5.c it can be seen that the magnetic induction has greater values than in Fig. 5.a where the field is produced only by PM. Conversely, in the differential compound Fig. 5.d, the magnetic field in the central pole and magnetic saturation in the vicinity poles are reduced in comparison to values in Fig.5 .a.

In case of additional compound, due to strong magnetic saturation of the stator core and middle pole (colored in yellow in Fig. 5.c), magnetic filed that closes through the ferromagnetic cylinder surrounding the field coil is reduced

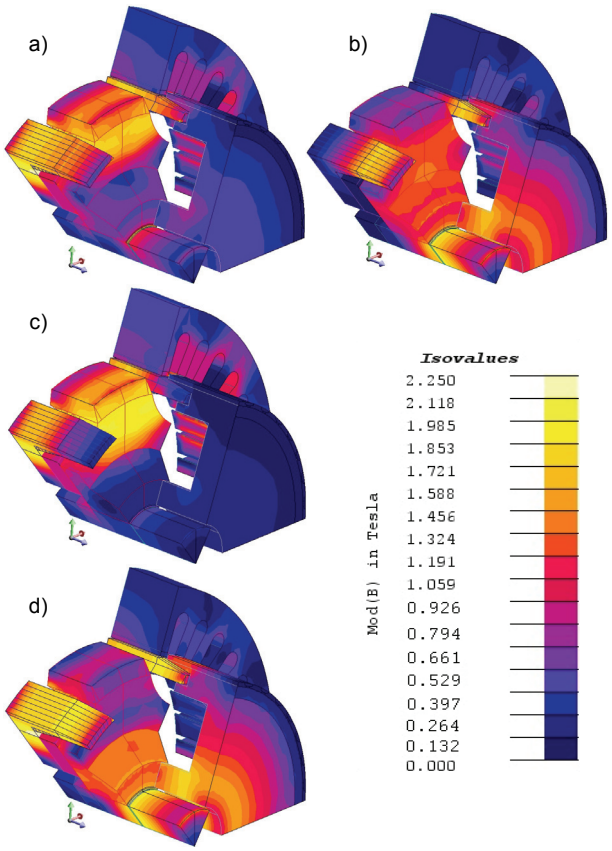

Fig. 5. Magnetic flux density map produced by: a. PM alone. b. Field coils at I_f = 3A; c. Hybrid additive excitation with I_f = 3A; d. Hybrid differential excitation with I_f = -3A

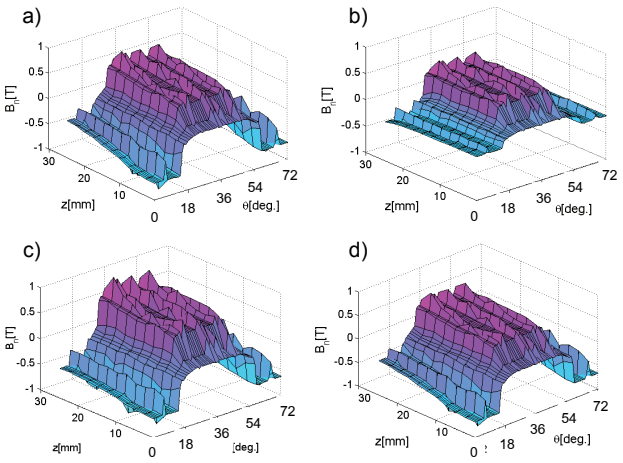

Fig.6. Radial flux density in the airgap produced by: a. PM alone. b. Field coils at I_f=3A; c. Hybrid additive excitation with I_f=3A; d.Hybrid differential excitation with I_f=-3A

(magnetic induction in blue in Fig. 5.c). In case of differential compound, Fig. 5.d, when there is noticeable lower magnetic flux density in the middle pole and no saturation, the magnetic field closing through the ferromagnetic cylinder is greater and causes saturation (magnetic induction colored from blue to yellow in Fig. 5.d).

Another important analysis regards the distribution of the radial magnetic flux density in the air-gap of the machine. In case of an additive compound, Fig. 6.c, the magnetic induction has almost same value in two consecutive poles and only a slight variation along the axial length of the machine. In case of a differential compound the average value of the magnetic flux density in two consecutive poles differs, and the variation along the axial direction is important. The origin of *z* axis in the plots shown in Fig. 6 is located in the mid cross section of the machine (the symmetry plan).

Also from Fig. 6 one can observe that the magnetic fluxes under two consecutive poles are not equal, the difference being larger when magnetic field is produced only by the field coil (in the absence of the permanent magnets), or by a differential compound. This uneven magnetic distribution is caused by the axial magnetic field which closes through the side ferromagnetic cylinders.

Further on, in order to compute the e.m.f. induced in a coil, a surface following the coil shape was considered, as seen in Fig. 4. The magnetic flux passing through this surface was computed for each of the four cases corresponding to the situations presented in Fig. 6, for successive rotor displacements between two consecutive poles. The flux time dependence is illustrated in Fig. 7. Consistent with the observation made regarding the non-symmetry of the magnetic induction under successive poles in Fig. 6, the flux-time curves are also asymmetrical,

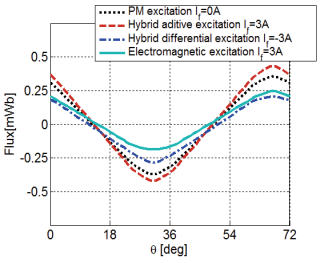

Fig.7. Flux of a stator winding coils according to the rotor position

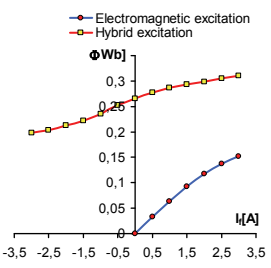

Fig.8. Magnetization characteristic

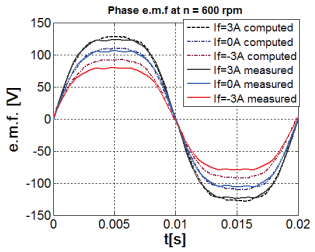

Fig. 9 Computed and measured waveforms of phase e.m.f. at n = 600 rpm

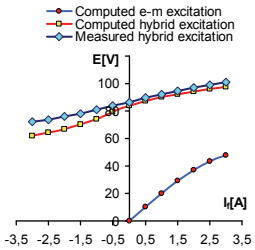

Fig. 10 No-load characteristic at 600 rpm

a higher offset being noticed when field is produced only by field current or in the case of a differential compound.

In order to determine machine's magnetic curve in Fig. 8, the waveforms from Fig. 7 were extended using periodicity. All fluxes corresponding to the coils of one-phase winding were added up. The relative position of the coils of one phase and the way they interconnect was determined from the winding scheme. As the number of coil sides of one phase winding under north are equal with those under south poles, the magnetic flux per phase against rotor position is symmetrical against the abscise.

Knowing the magnetic flux Φ_k per phase for each successive rotor position θ_k, and the angular velocity Ω, it was possible to compute the e.m.f at each moment $t_k = \theta_k / \Omega$ using relation (8):

$$e(t_k) = -p\frac{\Phi_{k+1} - \Phi_{k-1}}{2\Delta\theta}\Omega\,, \tag{8}$$

where $2\Delta\theta$ represents the angular displacement between position θ_{k-1} and θ_{k+1}. Using this algorithm the e.m.f. has been computed for rotor speed n = 600 rpm. Fig. 9 shows computed and experimentally determined e.m.f. corresponding to three different values of the field current (0A, 3A and -3A respectively). A difference between numerical and experimental results can be noticed in Fig. 9 for the differential compound (I_f = -3A).

Further on, Fig. 10 shows the computed and measured e.m.f. versus field current, i.e. the no-load characteristic at rotor speed n = 600 rms.

As in previous determinations, the numerical and experimental results are in accordance for additional compound, but differ slightly for differential compound (negative current in Fig.10). One explanation for the slight non-consistency could be that the magnetization characteristic of the ferromagnetic cylinder surrounding the field coil used in the numerical model did not reflect exactly that of the real material. Also the model did not consider eddy currents losses and their effect over the ferromagnetic cylinder magnetic properties due to heating.

Conclusions

Positioning the field coils in the stator was done with the purpose of eliminating contact slip rings. That generated a specific magnetic configuration of the hybrid machine.

The present analysis provides several important conclusions regarding the way of generating the magnetic field in this hybrid machine and how field closes through different parts of the magnetic circuit.

The magnetic flux density in the ferromagnetic cylinders surrounding the field coils, made to conduct magnetic field towards the air-gap, depends on the direction of the field current. In case of an additional compound, due to high magnetic saturation of the main pole, the field in the ferromagnetic cylinder is weak. Field gets stronger when a differential compound is used, for which magnetic field distribution inside machine is more balanced altogether, with less saturation. In the later case the magnetic flux density becomes higher in the ferromagnetic outer cylinders, and eddy current losses increase. Thus, when differential compound is used, the eddy currents that have been not considered in the numerical model can have a greater influence. This could also provide an explanation for the differences between numerical and measured values for the differential compound case.

The work has been co-funded by the Sectorial Operational Programme Human Resources Development 2007-2013 of the Romanian Ministry of Labour, Family and Social Protection through the Financial Agreement POSDRU/89/1.5/S/62557.

REFERENCES

[1] Cistelecan M.V., Popescu M., Melcescu L., "Electric machine with hybrid excitation without sliding contacts", Romanian patent RO-125062, issued 30 December 2010.

[2] Amara, Y.; Vido, L.; Gabsi, M.; Hoang, E.; Hamid Ben Ahmed, A.; Lecrivain, M.; , "Hybrid Excitation Synchronous Machines: Energy-Efficient Solution for Vehicles Propulsion," *Vehicular Technology, IEEE Trans.* on , vol.58, no.5, pp.2137-2149, Jun 2009.

[3] Kosaka, T.; Sridharbabu, M.; Yamamoto, M.; Matsui, N.;"Design Studies on Hybrid Excitation Motor for Main Spindle Drive in Machine Tools,"*Ind. Electr.,IEEE Trans. on* ,vol.57, no.11, pp.3807-3813, Nov. 2010.

[4] Syverson, Ch., Hybrid alternator, US Patent 6,236,134/2001.

[5] Demeter E., Nitigus V., Cistelecan M.V., Moraru A., Combined Excitation Alternator for Motor Vehicles, Romanian patent RO-00118347, issued 30 April 2003.

[6] Ifrim C., "Hybrid Brushless Electric Machines", US Patent 2002/0180297 A1/2002.

[7] Finken, T.; Hameyer, K.; , "Study of Hybrid Excited Synchronous Alternators for Automotive Applications Using Coupled FE and Circuit Simulations," *Magnetics, IEEE Transactions on* , vol.44, no.6, pp.1598-1601, June 2008

[8] Munteanu, A.; Simion, A.; Livadaru, L.; "Optimization study upon excitation pole shape of a hybrid synchronous generator," Power Electronics, Electrical Drives, Automation and Motion, 2008. SPEEDAM 2008. International Symposium on , vol., no., pp.1292-1296, 11-13 June 2008.

[9] Zhuoran Zhang; Yangguang Yan; Shanshui Yang; Zhou Bo; , "Principle of Operation and Feature Investigation of a New Topology of Hybrid Excitation Synchronous Machine," *Magnetics, IEEE Transactions on* , vol.44, no.9, pp.2174-2180, Sept. 2008.

[10] Chengfeng Yang; Heyun Lin; Jian Guo; Zhu, Z.Q.; , "Design and Analysis of a Novel Hybrid Excitation Synchronous Machine With Asymmetrically Stagger Permanent Magnet," *Magnetics, IEEE Transactions on* , vol.44, no.11, pp.4353-4356, Nov. 2008.

[11] Qi Zhang; Surong Huang; Guodong Xie; , "Design and Experimental Verification of Hybrid Excitation Machine With Isolated Magnetic Paths," *Energy Conversion, IEEE Transactions on* , vol.25, no.4, pp.993-1000, Dec. 2010.

[12] Cedrat, Flux® 10 User's Guide, Vol.1-5, 2007.

***Authors**: Lecturer Dr. Eng. Leonard MELCESCU, Electrical Machines Dept., Electrical Engineering Faculty, POLITEHNICA University of Bucharest, 313 Spl. Independentei, S-6, Bucharest, Romania, E-mail: leonard@amotion.pub.ro; Dr. Eng. Mihail V. CISTELECAN, Research Institute for Electrical Machines (ICPE-ME), 45 Tudor Vladimirescu, S-5, Bucharest, Romania,E-mail: mciste@yahoo.com, Lecturer Dr. Eng. Ovidiu CRAIU, Electrical Machines Dept., Electrical Engineering Faculty, POLITEHNICA University of Bucharest, 313 Spl. Independentei, S-6, Bucharest, Romania, E-mail: ocraiu@yahoo.com, Dr. Eng. Mihail POPESCU, Research Institute for Electrical Machines (ICPE-ME), 45 Tudor Vladimirescu, S-5, Bucharest, Romania, E-mail: pd_mihail@yahoo.com.*